Air-Promoted Adsorptive Desulfurization of Diesel Fuel Over Ti-Ce Mixed Metal Oxides

Jing Xiao
Clean Fuels and Catalysis Program, EMS Energy Institute, Pennsylvania State University, University Park, PA 16802

Dept. of Energy and Mineral Engineering, Pennsylvania State University, University Park, PA 16802

School of Chemistry and Chemical Engineering, South China University of Technology, Guangzhou 510640, China

Siddarth Sitamraju, Yongsheng Chen, Shingo Watanabe, and Mamoru Fujii
Clean Fuels and Catalysis Program, EMS Energy Institute, Pennsylvania State University, University Park, PA 16802

Dept. of Energy and Mineral Engineering, Pennsylvania State University, University Park, PA 16802

Michael Janik and Chunshan Song
Clean Fuels and Catalysis Program, EMS Energy Institute, Pennsylvania State University, University Park, PA 16802

Dept. of Energy and Mineral Engineering, Pennsylvania State University, University Park, PA 16802

Dept. of Chemical Engineering, Pennsylvania State University, 104 Fenske Laboratory, University Park, PA 16802

DOI 10.1002/aic.14647
Published online October 18, 2014 in Wiley Online Library (wileyonlinelibrary.com)

Air-promoted adsorptive desulfurization (ADS) of commercial diesel fuel over a Ti-Ce mixed oxide adsorbent in a flow system is investigated in this work. The fresh/spent adsorbents were characterized using X-ray absorption near edge structure spectroscopy. Results show that sulfoxide species are formed during air-promoted ADS over $Ti_{0.9}Ce_{0.1}O_2$ adsorbent. Adsorption selectivity of various compounds in fuel follows the order of dibenzothiophene sulfone > dibenzothiophene ≃ benzothiophene > 4-methyldibenzothiophene > 4,6-dimethyldibenzothiophene > phenanthrene > methylnaphthalene > fluorene > naphthalene. The high adsorption affinity of sulfoxide/sulfone is attributed to stronger Ti-OSR_2 than Ti-SR_2 interactions, resulting in significantly enhanced ADS capacity. Adsorption affinity was calculated using ab initio methods. For Ti-Ce mixed oxides, reduced surface sites lead to O-vacancy sites for O_2 activation for oxidizing thiophenic species. Low temperature is preferred for air-promoted ADS, and the Ti-Ce adsorbent can be regenerated via oxidative air treatment. This study paves a new path of designing regenerable adsorbents. © 2014 American Institute of Chemical Engineers *AIChE J*, 61: 631–639, 2015
Keywords: desulfurization, adsorption, metal oxides, diesel

Introduction

Diesel fuel has been considered as a preferable feedstock for hydrogen production for on-site and on-board fuel cell applications due to its high energy density and ready availability with existing infrastructures as well as safety and ease of production, delivery, and storage.[1] However, trace amounts of sulfur in diesel fuel cause poisoning of the reforming catalysts, water-gas-shift catalysts, and the electrodes in fuel cell systems.[2] Fuel cells require fuel with <1 part per million by weight of sulfur (ppmw-S) for efficient operation. Therefore, reducing the sulfur content is a key to utilize diesel fuel to produce hydrogen for on-board fuel cells. Currently, for the protection of the environment and human health,[3–5] the sulfur content in diesel fuel has been regulated to be less than 15 ppmw in the United States since 2006.[3,4] The regulation has imposed challenges on refineries using the traditional hydrodesulfurization (HDS) technology. HDS is highly efficient to remove thiols and sulfides but not efficient for the refractory thiophenic compounds in diesel fuel such as 4,6-dimethyldibenzothiophene (4,6-DMDBT).[3] The production of ultraclean fuel with <1 ppmw-S for fuel cell applications from HDS requires a much bigger catalyst bed, higher temperature and pressure, and more hydrogen input.[6] Therefore, ultradeep desulfurization of diesel fuel has become a more important research subject worldwide.

Additional Supporting Information may be found in the online version of this article.

Correspondence concerning this article should be addressed to C. Song at cxs23@psu.edu.

Adsorption desulfurization (ADS), based on the selective adsorption of organosulfur compounds over a solid adsorbent, has been considered a promising approach for ultradeep desulfurization. There are ongoing efforts to develop new adsorbents for desulfurization of liquid fuels, including π-complexation sorbents,[7,8] immobilized π-acceptor sorbents,[9] metal organic frameworks,[10,11] nickel-based sorbents,[12] carbon sorbents,[13] aluminosilicates,[14,15] and soft acid-supported sorbents.[16,17] Metal oxides show promising features for adsorption and catalysis due to their air-regenerability, adjustable composition, and functionalities as well as tunable textural properties.

Metal oxides have been extensively studied for hot coal gas desulfurization to remove hydrogen sulfide (H_2S) via high temperature sulfidation.[18–20] We previously reported that air can increase ADS capacity over a mixed $Ti_{0.9}Ce_{0.1}O_2$ adsorbent under ambient conditions through promotion of the chemical transformation of organosulfur compounds to sulfoxides.[21] Our density functional theory (DFT) calculations suggested that chemisorbed oxygen on the TiO_2 surface plays an important role for ADS[22] providing an O-source for chemical transformation of sulfur compounds over metal oxides. Questions remain as to the impact of thiophenic constituents on sulfoxide formation and ADS selectivity, adsorption modes, and thermodynamics over Ti-Ce mixed metal oxides and the effect of temperature on adsorption capacity and adsorbent regenerability.

In this work, air-promoted ADS of commercial diesel fuel over Ti-Ce mixed metal oxide adsorbents is studied systematically. Adsorption capacity and selectivity were determined using a fixed-bed flow system. Adsorption affinity of various compounds in fuel was calculated using DFT methods. The fresh/spent/regenerated adsorbents were characterized using X-ray absorption near-edge structure (XANES) techniques. The adsorption selectivity of various compounds in fuel as well as oxidized thiophenic species (sulfoxide/sulfone) over the mixed $Ti_{0.9}Ce_{0.1}O_2$ adsorbent was compared and corroborated with the *ab initio* calculations. Possible active sites on Ti-Ce mixed metal oxides for catalytic ADS mechanism were identified by Ce $M_{4,5}$-edge XANES characterization. The temperature effect on the air-promoted ADS over the mixed $Ti_{0.9}Ce_{0.1}O_2$ adsorbent was investigated. The regeneration of spent mixed $Ti_{0.9}Ce_{0.1}O_2$ adsorbent was also examined.

Experimental

Syntheses of metal oxides

The TiO_2, CeO_2, $Ti_{0.5}Ce_{0.5}O_2$, and $Ti_{0.9}Ce_{0.1}O_2$ adsorbents were synthesized by a urea coprecipitation method, as described elsewhere.[22] All the chemicals were purchased from Sigma-Aldrich and were used as received without further purification.

Fuels

A commercial low-sulfur diesel fuel containing 14.5 ppmw-S from British Petroleum was used, and its composition was described in our earlier paper.[13] A model diesel fuel (MDF) was prepared to evaluate the adsorption selectivity of different compounds over the mixed $Ti_{0.9}Ce_{0.1}O_2$ adsorbent. The model fuel contained the same molar concentration (3.12 E − 3 mol/kg) of benzothiophene (BT, 99%), dibenzothiophene (DBT, 98%), 4-methyldibenzothiophene (4-MDBT, 96%), 4,6-DMDBT, (97%), dibenzothiophene sulfone ($DBTO_2$, 97%), indole (≥99%), naphthalene (Nap, 99%), fluorene (Flu, 98%), 2-methylnaphthalene (MNap, 97%), and phenanthrene (Phe, 98%). Tert-butylbenzene (99%) of 8 wt %, 2 wt % of furan (98%), 45 wt % of *n*-decane (≥99%), and 45 wt % of hexadecane (≥99%) were added into the MDF as the solvents. 3.12 E − 3 mol/kg (3.12 μmol/g) of *n*-tetradecane (≥99%) was added as an internal standard for adsorption selectivity calculation. All the chemicals were purchased from Sigma-Aldrich, and were used as received.

Flow ADS experiments

ADS runs were performed in a fixed-bed flow system with a stainless steel column (0.0046 m I.D. × 0.075 m length [4.6 mm I.D. × 75 mm length]). 6 E − 4 kg (0.6 g) of the dried adsorbent was packed into a stainless steel column and then predried *in situ* under an air flow rate of 10 cc/min (1.67 E − 7 m^3/s) at 393 K for 7.2 E 3 s (2 h). The commercial diesel fuel (or the model fuel) was fed with a high performance liquid chromatography (HPLC) pump into the column at a liquid hourly space velocity of 4.8 h^{-1} corresponding to a flow rate of 0.1 cc/min (1.67 E − 9 m^3/s). Air was fed into the flow system during the ADS test through a mass flow controller. The air was pre-mixed with the fuel before feeding into the ADS column. The effluent fuel was periodically sampled at an interval of 900–1200 s (15–20 min) for analyses.

Fuel analyses

An ANTEK 9000 series sulfur analyzer was used to analyze the total sulfur concentration of the treated fuel samples. The sulfur compound compositions in the initial and treated fuels were determined using a Hewlett Packard gas chromatograph equipped with a sulfur-selective pulsed flame photometric detector (GC-PFPD). A Hewlett Packard 5890 series II gas chromatograph with a capillary column (XTI-5, Restek, bonded 5%, 30 m length × 2.5 E − 4 m I.D. × 2.5 E − 7 m film thickness [30 m × 0.25 mm I.D. × 0.25 μm]) and a split mode injector (ratio: 100:1) were used. Ultrahigh-purity helium was used as the carrier gas. The oven temperature was initially set at 393 K and after injection ramped at 0.1 K/s (6°C/min) to 443 K, followed by another ramp at 0.33 K/s (20°C/min) from 443 to 563 K and then held at 563 K for 300 s. Both injector and detector temperature in GC-PFPD analysis were kept at 563 K.

For the adsorption selectivity study, compounds in treated MDF samples were analyzed by a gas chromatograph (Varian CP 3800) equipped with a flame ionization detector. The compounds were separated by a VF-5 ms capillary column (30 m length × 2.5 E − 4 I.D. × 2.5 E − 4 m film thickness (30 m × 0.25 mm × 0.25 mm). Helium was used as a carrier gas at a flow rate of 1.0 cc/min (1.67 E − 8 m^3/s). The oven temperature program was the same as above.

To facilitate the quantitative discussion of the adsorptive selectivity, a relative selectivity factor was used in this study, which is defined as

$$\alpha_{i-n} = Cap_i / Cap_n \quad (1)$$

where Cap_i is the adsorptive capacity of compound "i" corresponding to the breakthrough point and Cap_n is the adsorptive capacity of the reference compound, naphthalene (Nap), corresponding to its breakthrough point. As we used the

kinetic breakthrough capacities instead of the equilibrium capacity in Eq. 1, the defined selectivity factor does not indicate equilibrium selectivity.[23]

Adsorbent characterization

Sulfur K-edge XANES spectroscopic measurements of spent ADS adsorbents were performed at beamline 9-BM/XOR of the Advanced Photon Source at the Argonne National Lab. The storage ring was operated with an electron beam of 6.75 E 11 kJ/mol (7 GeV) and an electron current of 0.1 A in a top-up mode. The monochromator was double-crystal Si(111), and the XANES spectra were collected in fluorescence mode with a Si DRIFT 4-element detector (Vortex). Air absorption was controlled by the use of helium purging in the incident light path and the sample chamber, which were separated by a 5 E − 6 m (5 micron) thick polycarbonate window. The monochromator crystals had an energy resolution of ~28.93 kJ/mol (0.3 eV) at 2.41 E 5 kJ/mol (2.5 keV). Harmonics were rejected by use of a Rh-coated flat mirror in the experimental station. The beam was focused to as pot size of ~1 E − 3 m (1 mm) in the horizontal and vertical directions by the use of a Rh-coated toroidal mirror.[24] To avoid further oxidation, the spent adsorbent was sealed in the adsorption column after an ADS experiment and then transferred to and sealed in a sample cell with a propylene window, which allows for XANES measurements of liquid or volatile samples. Energy calibration was accomplished by setting the edge energy of elemental sulfur to 2.38 E 5 kJ/mol (2472.0 eV). To establish the relationship between the edge energy and oxidation state, reference compounds DBT, 4,6-DMDBT, and $DBTO_2$, were measured as received from Sigma-Aldrich. Up to five scans were collected and averaged to improve the signal to noise ratio. XANES data were processed using the Athena software package.[25]

Ce $M_{4,5}$-edge XANES measurement was performed at beamline U7A of the National Synchrotron Light Source at Brookhaven National Laboratory, Upton, NY. Detailed information about the experimental setup can be found elsewhere.[26] The storage ring was operated with an electron beam energy of 7.72 E 10 kJ/mol (800 MeV) and an average current of 0.6 A. XANES spectra were collected in partial electron yield mode. The energy range for Ce $M_{4,5}$-edge XANES measurements was from 8.20 E 4 to 8.97 E 4 kJ/mol (850–930 eV). The energy interval was 9.64 kJ/mol (0.1 eV) in the critical region and 48.22 kJ/mol (0.5 eV) in the other regions. Samples were pressed onto a copper tape uniformly and no cracks were observed. The samples were tenths of a millimeter thick so that no interference from the adhesive on the copper tape was expected. The samples were placed in an ultrahigh vacuum chamber maintained at a pressure lower than 10^{-8} Pa.[27] The Ce $M_{4,5}$-edge XANES spectra were processed using the Athena package.

Computational analysis

Dipole Moment Calculations. Dipole moments of the adsorbent molecules were calculated using the Gaussian 09 package. All the molecules were optimized with a 6−31+G(d) basis set, and a B3LYP exchange-correlation functional.

Adsorption Energy Calculations. Adsorption energy calculations were performed using the Vienna Ab initio Simulation Program (VASP[28–30]). The wave functions of the core electrons were represented using the projector augmented wave[31] method. A cutoff energy of 4.34 E 4 kJ/mol (450 eV) was used for the plane wave basis sets for the valence electrons of Ti, Ce, O, C, S, and H. The generalized gradient approximation of the Perdew–Wang 91[32] functional was used for the determination of the exchange and correlation potential. A 3×3×1 Monkhorst-Pack k-point mesh[33] was used for all surface calculations. The electronic self-consistent field was converged to 9.64 E − 3 kJ/mol (1×10^{-4} eV) and the structure was optimized until the forces on all atoms were less than 4.82 E − 10 kJ mol^{-1} m^{-1} (0.05 eV $Å^{-1}$). A subset of the model systems were optimized by converging the self consistent field (SCF) cycle to 9.64 E − 4 kJ/mol (1×10^{-5} eV) and until the forces on the atoms were less than 1.93 E − 10 kJ mol^{-1} m^{-1} (0.02 eV $Å^{-1}$). The absolute energies differ by less than 0.1 kJ mol^{-1}. Dipole corrections were included in all the calculations to minimize the possible inaccuracies in the total energy due to the simulated slab-to-slab interactions (VASP keywords IDIPOL = 3, LDIPOL = TRUE).

Electrons in localized 4f states of reduced ceria cannot be accurately represented by DFT, due to a self-interaction error for highly correlated systems. DFT-U has been used with U = 4.82 E 2 kJ/mol (5 eV) for Ce 4f states as suggested in the literature.[34]

The DFT-D2 method of Grimme[34] has been used to represent the nonbonding interactions within the systems. The lack of C_6 parameters for the later part of the periodic table, most notably the actinide series led us to hypothesize that at low concentrations of dopants, the magnitude of the dispersion energy added varies due to the change in the size of the adsorbate and not due to the chemical composition of the surface itself. Adsorption energies are calculated as the energy difference between the adsorbate-adsorbent system and the two isolated systems.[35]

Model Construction. As considered in our previous work, a titania anatase unit cell consisting of four Ti atoms and eight O atoms was used for bulk optimization. The (001) surface, which is the most reactive low index surface, is considered. The surface slab has four layers of Ti-O atoms, with the top two layers unconstrained during structural optimization and the bottom two layers frozen to replicate the behavior of a bulk crystal. A 2 × 2 supercell ($Ti_{16}O_{32}$) was used for all the calculations. For the Ce-doped systems, a single Ti atom at the surface was replaced by a Ce atom ($Ti_{15}CeO_{32}$).

Results and Discussion

Effect of air on ADS over $Ti_{0.9}Ce_{0.1}O_2$ adsorbent

Figure 1 shows the breakthrough (B.T.) capacities for total sulfur compounds at breakthrough concentrations of 1 ppmw-S and 3 ppmw-S from the commercial diesel over a $Ti_{0.9}Ce_{0.1}O_2$ adsorbent at various air flow rates. The breakthrough capacity first increases with air flow rate up to 10 cc/min (1.67 E − 7 m^3/s) and then remains constant for higher air flow rates up to 40 cc/min (6.67 E − 7 m^3/s). By introducing 10 cc/min (1.67 E − 7 m^3/s) of air during ADS, desulfurization capacity over $Ti_{0.9}Ce_{0.1}O_2$ mixed oxides increased ninefold from 2.5 kilogram of fuel per kilogram of sorbent (2.5 kg-F/g-sorb or 2.5 g-F/g-sorb) to 22.5 kg-F/kg-sorb (22.5 g-F/g-sorb) at a breakthrough concentration of 1 ppmw-S. The results indicate that air significantly promotes ADS over the $Ti_{0.9}Ce_{0.1}O_2$ mixed oxide adsorbent.

Adsorption selectivity of $Ti_{0.9}Ce_{0.1}O_2$ adsorbent

In our previous communication,[21] sulfoxides were identified as the predominant sulfur species on the spent

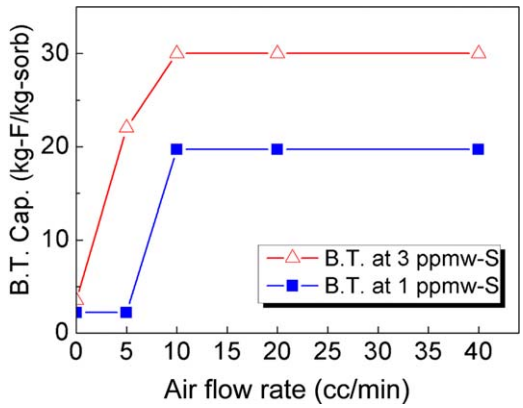

Figure 1. Breakthrough (B.T.) capacities for total sulfur compounds at breakthrough concentrations of 1 and 3 ppmw-S from the commercial diesel over $Ti_{0.9}Ce_{0.1}O_2$ adsorbent as a function of air flow rates.

[Color figure can be viewed in the online issue, which is available at wileyonlinelibrary.com.]

$Ti_{0.9}Ce_{0.1}O_2$ mixed oxides adsorbent, suggesting oxygen molecule in air initiates or promotes the chemical transformation of the refractory sulfur compounds to sulfoxides. The sulfoxides were formed on the surface of the adsorbent via catalytic air oxidation of fuel; the formed sulfoxides remained on the surface of Ti-Ce metal oxides rather than in the bulk liquid. To understand the contribution of chemically transformed sulfoxide species to ADS, adsorption selectivity of different compounds in a model fuel over the $Ti_{0.9}Ce_{0.1}O_2$ adsorbent was studied. Figure 2 shows the breakthrough curves of different compounds in a model fuel. These breakthrough curves were measured over the $Ti_{0.9}Ce_{0.1}O_2$ adsorbent without air addition to the fuel. $DBTO_2$ was used instead of the commercially unavailable dibenzothiophene sulfoxide (DBTO) because of the similar skeletal structure.

The adsorbent initially has capacity for many of the compounds, but as the bed progresses toward saturation, strongly adsorbing compounds with higher affinities displace the weakly adsorbed species. The progression of breakthrough of each species with time can be used to measure their relative affinity, with later breakthrough indicating a greater adsorption selectivity for a compound. The first breakthrough species were aromatic compounds, including Nap, Flu, MNap, and Phe, which gave breakthrough capacities of <5 kg-F/kg-sorb. The second set of breakthrough species were the nonoxidized sulfur species, including DMDBT, BT, MDBT, and DBT, which gave breakthrough capacities of <15 kg-F/kg-sorb. In contrast, the fully oxidized sulfur species $DBTO_2$ had a breakthrough capacity of around 25 kg-F/kg-sorb. The last breakthrough species was indole, which gave the highest breakthrough capacity of around 70 kg-F/kg-sorb. In comparison to nonoxidized sulfur compounds, especially DMDBT, the oxidized sulfur compound $DBTO_2$ showed a much higher ADS breakthrough capacity over the $Ti_{0.9}Ce_{0.1}O_2$ adsorbent, indicating a much stronger adsorption affinity.

After passing through the saturation point ($C/C_0 = 1$), the outlet concentration of some compounds, including the aromatics and nonoxidized sulfur compounds, increases well above the initial concentration in the model fuel ($C/C_0 > 2.0$) and then decreases gradually to the initial concentration ($C/C_0 = 1$). This phenomenon is explained by the reversible nature of adsorption, and these compounds' lower adsorptive affinity than the subsequent breakthrough compounds. The initially adsorbed compounds with lower adsorptive affinity are replaced by the compounds with higher adsorptive affinity.[23] The observed "kicking-off" phenomenon further suggested that the adsorptive affinity followed the order of indole > DBT sulfone >> nonoxidized sulfur compounds > aromatic compounds.

The adsorption selectivity factor and the adsorption capacity of the studied compounds over the $Ti_{0.9}Ce_{0.1}O_2$ adsorbent are listed in Tables 1 and 2. $DBTO_2$ shows higher adsorption selectivity than nonoxidized sulfur compounds, and adsorption selectivity shows a general correlation with adsorbate dipole moment (Table 3). The high dipole magnitude of $DBTO_2$ can be attributed to the presence of the electronegative oxygen. It should be noted that the sulfur compounds observed on spent $Ti_{0.9}Ce_{0.1}O_2$ adsorbent were sulfoxides rather than sulfones. The adsorption affinity of DBTO may be lower than $DBTO_2$, but certainly higher than DMDBT, as the dipole magnitude follows the order of $DBTO_2$ (5.453 D) > DBTO (4.182 D) > DMDBT (0.764 D). The selectivity results suggest that strongly adsorbing sulfoxide/sulfone species over the $Ti_{0.9}Ce_{0.1}O_2$ surface from a chemical transformation of weakly adsorbing sulfur species in the fuel is the reason for significantly enhanced ADS capacity.

The selectivity of nonoxidized sulfur compounds follows the order of DBT > MDBT > DMDBT, confirming the presence of $-CH_3$ next to sulfur atom on nonoxidized sulfur compounds hindered ADS over the $Ti_{0.9}Ce_{0.1}O_2$ adsorbent. This trend suggests the adsorption of nonoxidized sulfur compounds over the $Ti_{0.9}Ce_{0.1}O_2$ adsorbent is likely through the sulfur atom, which is sterically hindered by the methyl groups, similar as ADS over supported nickel.[13] In contrast, the adsorption of sulfone over the $Ti_{0.9}Ce_{0.1}O_2$ adsorbent is likely through oxygen atom, which is not sterically hindered by the $-CH_3$ groups due to its out-of-plane configuration and greater distance of the ring from the surface. This study offers evidence for the results from DFT calculations reported by our group[35] before.

A high adsorption capacity and selectivity of indole was observed, significantly higher than $DBTO_2$. Indole, however, shows a lower dipole moment (2.004 D) than $DBTO_2$ (5.453 D) as listed in Table 3. Indole has a bifunctional electronic structure,[37] acting as an electron donor because of the conjugated pi system and as an electron acceptor due to the

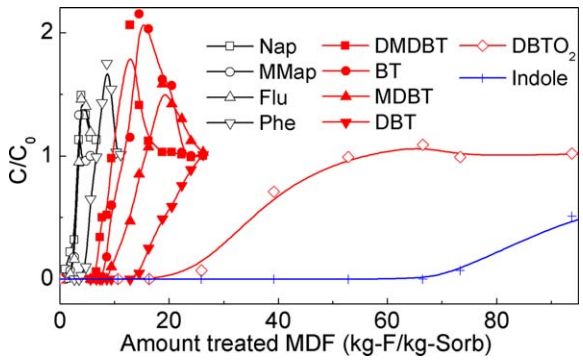

Figure 2. Breakthrough curves of different compounds over the $Ti_{0.9}Ce_{0.1}O_2$ adsorbent from the model fuel at 298 K.

[Color figure can be viewed in the online issue, which is available at wileyonlinelibrary.com.]

Table 1. Adsorption Selectivity Factor Relative to Naphthalene for Each Compound in MDF over the $Ti_{0.9}Ce_{0.1}O_2$ Adsorbent and Adsorption Energies in kJ mol^{-1}

	Nap	Flu	MNap	Phe	DMDBT	BT	MDBT	DBT	$DBTO_2$	Indole	DBTO[a]
Experiment	1	1.88	1.88	4.76	6.68	7.74	9.44	11.14	25.90	73.31	NA
E_{ads}	−2.1	−4.2	−3.0	−7.5	−15.6	−31.8	−27.6	−32.8	−36.7	–	−85.8
E_{ads}(DFT-D)	−41.5	−56.5	−46.5	−55.7	−71.6	−88.2	−79.4	−97.3	−88.8	–	−260.4

[a]DBTO is not available for testing experimentally.

hydrogen bonded to nitrogen. Therefore, indole can behave as a weak base due to the basicity of the N atom and as a weak acid due to the H—N-bond.[38] The presence of nitrogen compounds in fuel might suppress ADS over the $Ti_{0.9}Ce_{0.1}O_2$ adsorbent due to competitive adsorption. A combination of two or more adsorbent beds in an ADS process may further improve the ultradeep desulfurization process.

DFT studies of adsorption modes and thermodynamics

DFT was used to study the preferred modes of adsorption of the different adsorbates on the surface and also to evaluate the adsorption thermodynamics. Our previous work reported that Ce-doping into anatase increased the exposure of the (001) facet[39] and that the doped (001) surface was the most reactive low index surface. We, therefore, consider adsorption to the (001) surface. All the molecules used in the model fuel were considered as possible adsorbates. Adsorption energies calculated with DFT and DFT-D method are included in Table 1. The dispersion correction leads to much stronger adsorption, but does not significantly change the trends among compounds.

As with the pure anatase surfaces, adsorption of the sulfur containing compounds on Ce-doped surfaces occurs due to electron transfer between the sulfur atom in the adsorbate and the surface metal atoms. The preferred site of adsorption in the binary system is the Ce atom. The extent of electron transfer from the S atom to the Ce is larger than from the S atom to a surface Ti atom. For a 4,6-DMDBT molecule, the adsorption energy (DFT-D energies are compared, as dispersion is needed to get significant adsorption information) on the pure surface is −60.18 kJ/mol (−0.624 eV), but the adsorption energy on the Ce-doped surface is −71.56 kJ/mol (−0.742 eV). The increased adsorption strength corresponds to increased electron transfer between the adsorbate and the active site of the adsorbent. Bader charge analysis of the S atom in the ring shows that the charge of the S atom in the DMDBT molecule is −0.14. On interaction with the pure TiO_2 surface, the S atom becomes less negative due to the electron transfer and has a charge of −0.12. On interaction with a doped surface, however, the S atom has a charge of −0.07, suggesting more electron transfer to the Ce dopant atom on the surface. The larger size of the Ce atom makes it possible for the adsorbate to adsorb without being situated very close to the surface, thereby mitigating the effect of steric hindrance.

Figure 3 shows the preferred adsorption modes of various benzothiophenic derivatives on the (001) surface. The adsorption strength follows the trend of steric hindrance as DMDBT < MDBT < DBT, which is consistent with the adsorption selectivity order. The substituted DBT molecules adsorb weaker than the DBT molecules. The adsorption energy trends among these species are unchanged between values with and without dispersion corrections.

The adsorption energies of the hydrocarbons are less exothermic than the adsorption energies of the sulfur containing compounds as suggested in Table 1. Figure 4 shows the optimized adsorbed configuration of naphthalene and fluorene on the Ce-doped TiO_2 (001) surface. The preferred interaction mode of the hydrocarbons is through pi electron transfer from the ring to the surface metal atoms. The adsorbate molecule is adsorbed parallel to the surface in a planar configuration, facilitating the interaction of the conjugated π electrons easier.

The DFT calculated adsorption energies of the hydrocarbons on both the TiO_2 and the Ce-doped TiO_2 are close to zero. Addition of dispersion interactions strengthen the adsorption, suggesting that Van Der Waal's forces and importantly the size of the adsorbate plays a major role in determining the strength of adsorption. Larger molecules like fluorene and Phe adsorb stronger than naphthalene, solely due to the increased size.

Sulfone species show stronger adsorption than nonoxidized thiophenic species, as indicated in the experimental adsorption selectivity results. Adsorption occurs through interaction of the oxygen atoms in the sulfone and the surface metal atoms (Figure 3c). As with the unoxidized sulfur compounds, Ce doping promotes the adsorption of sulfones to the surface.

The trend of adsorption strength on the (001) surface is: $DBTO_2 > DBT \simeq BT > MDBT > DMDBT >$ Phe > MNap > Flu > Nap. The trend is in close agreement with the trend of adsorption capacities observed experimentally. Adsorption calculations were also carried out for the DBTO molecule on the (001) surface (Figure 3f). The sulfur in this case is bound to one oxygen atom, which in turn bonds with the Ce atom on the surface. It has the strongest adsorption strength of all the adsorbates, although the instability of the gas phase sulfoxide makes direct comparison of adsorption energies difficult.

Effect of Ce dopant into TiO_2 on air-promoted ADS

Sulfur K-edge XANES. $Ti_{0.9}Ce_{0.1}O_2$ mixed metal oxides showed a significantly higher adsorption capacity compared

Table 2. Adsorption Capacities (mol/kg) for Each Compound in the Model Fuel over the $Ti_{0.9}Ce_{0.1}O_2$ Adsorbent

$Ti_{0.9}Ce_{0.1}O_2$	Nap	Flu	MNap	Phe	DMDBT	BT	MDBT	DBT	$DBTO_2$	Indole
Breakthrough	0.003	0.006	0.006	0.015	0.021	0.024	0.030	0.035	0.081	0.229
Saturation	0.008	0.009	0.009	0.017	0.025	0.030	0.043	0.060	0.149	>0.312
Net	0.005	0.007	0.007	0.012	0.014	0.018	0.030	0.060	0.149	>0.312

Table 3. Dipole Magnitude of Different Sulfur/Nitrogen Compounds Calculated with DFT (B3LYP/6–31+G(d))

Compound	BT	DBT	MDBT	DMDBT	DBTO	$DBTO_2$	Indole
Dipole moment (*D*)	0.665	0.803	0.476	0.138	4.741	5.743	2.004[36]

to single metal oxides of TiO_2 and CeO_2 in air-promoted ADS in our communication.[21] To understand the variation on sulfur chemistry over mixed and single oxides, sulfur K-edge XANES characterization was used to identify sulfur species on both mixed and single oxides. Figure 5 shows sulfur K-edge XANES spectra of the spent adsorbents, including TiO_2, CeO_2, and $Ti_{0.9}Ce_{0.1}O_2$. Sulfoxides[40] were detected only on the spent $Ti_{0.9}Ce_{0.1}O_2$, but not on the spent single TiO_2 and CeO_2 metal oxides, suggesting the mixed $Ti_{0.9}Ce_{0.1}O_2$ adsorbent demonstrates a unique functionality to activate oxygen in air for the transformation of organosulfur species to sulfoxides in fuel at room temperature.

Ce $M_{4,5}$-edge XANES. In the mixed Ti-Ce metal oxides, the oxidation states of Ce can vary due to the distorted crystalline structure. To investigate the oxidation states of the Ce dopant, Ce $M_{4,5}$-edge XANES was carried out on the mixed $Ti_{0.9}Ce_{0.1}O_2$ metal oxides, as well as the single CeO_2 metal oxides. Two stable oxidation states, +3 and +4, could be detected in cerium-containing metal oxides. The Ce $M_{4,5}$ XANES spectra arise from the transitions of 3d electrons into the unoccupied 4f states.[41] In the XANES spectra, Ce^{3+} and Ce^{4+} can be distinguished by their peak shapes and positions, and M5/M4 intensity ratio.[42] Supporting Information Figure S1 shows the Ce $M_{4,5}$-edge XANES spectra of the standard Ce^{3+} and Ce^{4+}. M5/M4 ratios in Ce $M_{4,5}$-edge XANES spectra was used to assess Ce^{3+}/Ce^{4+} ratio in oxides as reported in the literature.[41] M5/M4 ratio (1.18) for Ce^{3+} is higher than that for Ce^{4+} (0.73). Additionally, on the right side of major M4 and M5 peaks, a satellite peak appears on the XANES spectrum of Ce^{4+} rather than that of Ce^{3+}. Figure 6 shows the Ce $M_{4,5}$-edge XANES spectra of $Ti_{0.9}Ce_{0.1}O_2$ and CeO_2, as well as $Ti_{0.5}Ce_{0.5}O_2$ for comparison. The Ce^{3+} ratio in the Ti-Ce mixed metal oxides follows an order of $Ti_{0.9}Ce_{0.1}O_2$ (0.889) > $Ti_{0.5}Ce_{0.5}O_2$ (0.876) > lab-urea-precipitated CeO_2 (0.843), suggesting higher portions of Ce^{3+} in the Ti-Ce mixed metal oxides, consistent with the results in our previous X-ray photoelectron spectroscopy (XPS) study.[22] The characterization results consolidate that surface O-vacancies and their associated 3+ metal centers can act as active sites for O_2 activation and sulfoxide formation, as proposed in our DFT study.[21] It should be noted that even though Ce^{3+} was also presented in the lab-urea-precipitated CeO_2 (M5/M4 ratio of 0.843), low ADS capacity was observed. The lattice oxygen in the CeO_2 crystal is tricoordinated. An oxygen molecule has two O atoms which need to be bound with three surface Ce atoms (a vacancy in CeO_2 leaves three unsaturated Ce atoms),[43,44] which makes it difficult to adsorb and activate O_2 molecule. Therefore, O_2 molecule on CeO_2 is not as activated as it is on Ti-Ce surfaces, where an incoming O_2 molecule can bind with two unsaturated atoms. The detailed mechanism is further illustrated in our DFT work.

Effect of adsorption temperature on air-promoted ADS

Figure 7 shows the breakthrough curves of the $Ti_{0.9}Ce_{0.1}O_2$ adsorbent for sulfur compounds from the diesel fuel at 473, 373, 353, 323, and 298 K. By increasing the adsorption temperature, ADS capacity decreases, suggesting high

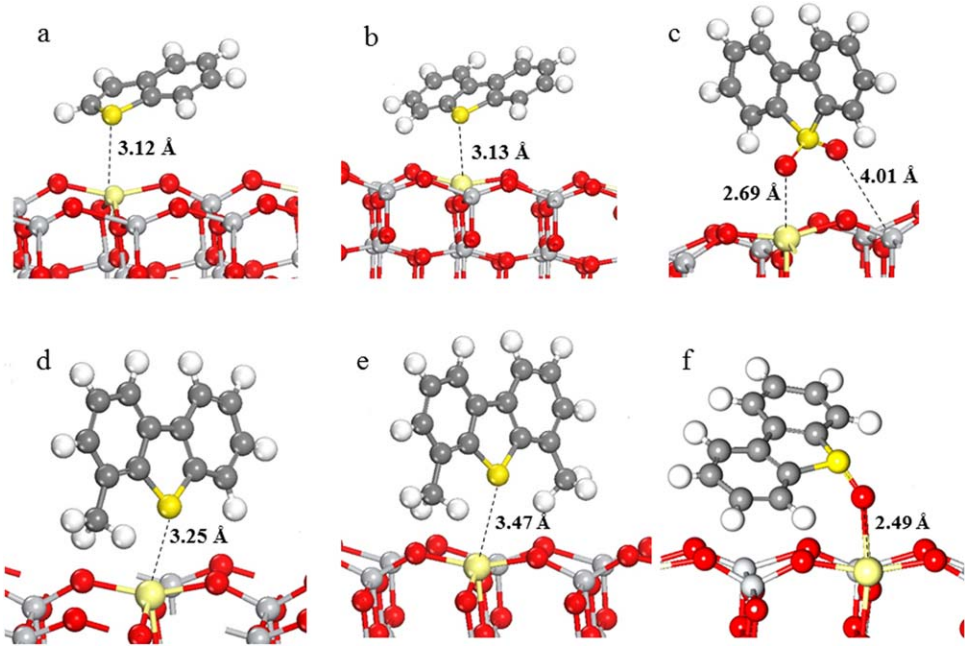

Figure 3. Adsorption configurations of BT and its derivatives over a Ce-doped TiO_2 (001) surface.(a) BT, (b) DBT, (c) DBT sulfone, (d) 4-MDBT, (e) 4,6-DMDBT; (f) DBTO; Ce, yellow; C, dark gray; H, white; Ti, light gray; O, red; S, dark yellow.

[Color figure can be viewed in the online issue, which is available at wileyonlinelibrary.com.]

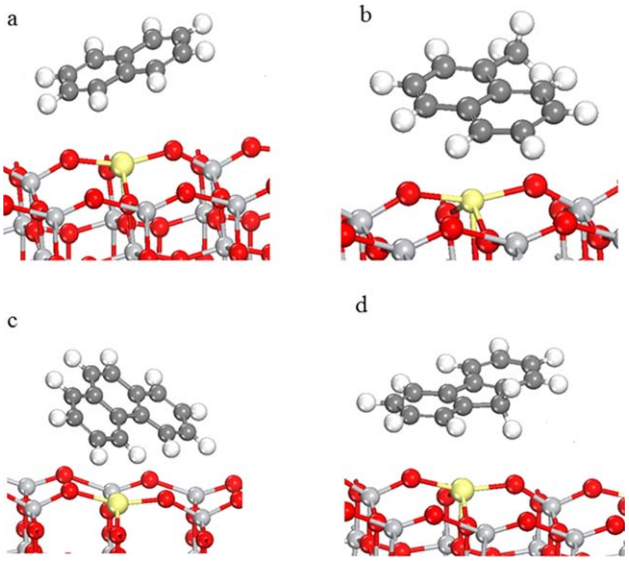

Figure 4. Adsorption configurations of hydrocarbons in model fuel over a Ce-doped TiO_2(001) surface. (a) Naphthalene, (b) Methylnaphthalene, (c) Phenanthrene, (d) Fluorene; Ce, yellow; C, dark gray; H, white; Ti, light gray; O, red.

[Color figure can be viewed in the online issue, which is available at wileyonlinelibrary.com.]

temperature conditions are not preferred for air-promoted ADS. In the temperature range studied, the optimal temperature for this process was 298 K. It is worth noting that no sulfoxides were detected in the treated fuels after breaking through at high temperatures, suggesting desorption of sulfoxides from the $Ti_{0.9}Ce_{0.1}O_2$ surface is not the reason for the decreased ADS capacity at higher temperatures. That is to say, reduced amount of sulfoxides are formed at increased ADS temperatures considering the two main steps (sulfoxide formation and sulfoxide adsorption) of air-promoted ADS. This can be attributed to the decreased amount of superoxide species formed on the $Ti_{0.9}Ce_{0.1}O_2$ surface at higher temperature in the presence of air. In another approach of ultradeep ADS of diesel fuel over TiO_2-CeO_2/MCM-48 adsorbent under ambient conditions we proposed,[45] peroxides are generated in fuel during air feeding under light irradiation before ADS, and the generated peroxides further oxidize and adsorb sulfur compounds over MCM-48 supported TiO_2-CeO_2. In contrast, during the air-promoted ADS process, it is likely the superoxide species formed on the unsupported $Ti_{0.9}Ce_{0.1}O_2$ surface due to O_2 in air governs the ADS capacity. It was also noted that there was no visible color change between the initial and desulfurized fuels, suggesting the oxygen content in the fuel increased negligibly and a high degree of oxidation of the sulfur containing compounds in the fuel.

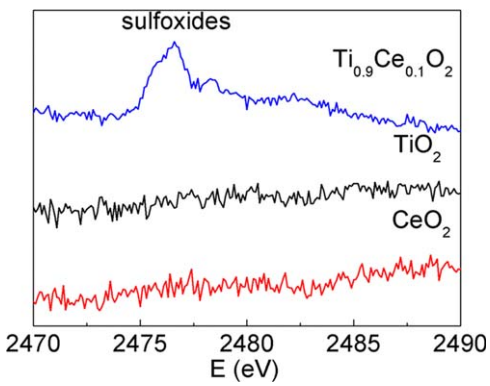

Figure 5. Sulfur K-edge XANES spectra of the spent TiO_2, CeO_2, and $Ti_{0.9}Ce_{0.1}O_2$ adsorbent after 1 h time-on-stream on the diesel fuel.

[Color figure can be viewed in the online issue, which is available at wileyonlinelibrary.com.]

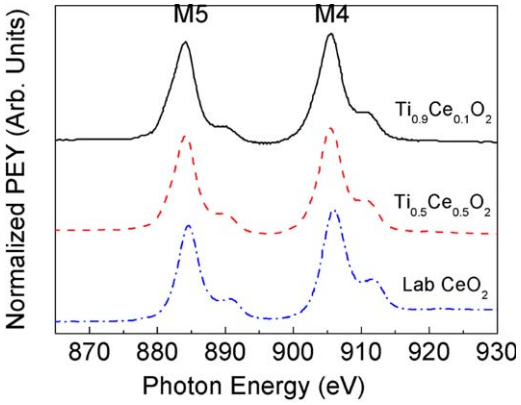

Figure 6. Ce $M_{4,5}$-edge XANES spectra of $Ti_{0.9}Ce_{0.1}O_2$, $Ti_{0.5}Ce_{0.5}O_2$, and CeO_2.

[Color figure can be viewed in the online issue, which is available at wileyonlinelibrary.com.]

Adsorbent regeneration

The regeneration of spent $Ti_{0.9}Ce_{0.1}O_2$ adsorbent was performed by oxidative air treatment. Figure 8 shows the breakthrough capacity of the $Ti_{0.9}Ce_{0.1}O_2$ adsorbent in the first three regeneration cycles by oxidative air treatment at 673 K. Regenerated $Ti_{0.9}Ce_{0.1}O_2$ adsorbent shows a comparable ADS capacity of 22.5, 20.2, 17.3 kg-F/kg-sorb in the first three cycles, indicating that the adsorption capacity can be recovered by oxidative air treatment. It further suggests that the active sites for air-promoted ADS on the $Ti_{0.9}Ce_{0.1}O_2$ adsorbent can be regenerated during oxidative air treatment. Meanwhile, the adsorption capacity drops gradually after cycles of regeneration, indicating partial loss of active sites accompanying the regeneration of the $Ti_{0.9}Ce_{0.1}O_2$ adsorbent via oxidative air treatment.

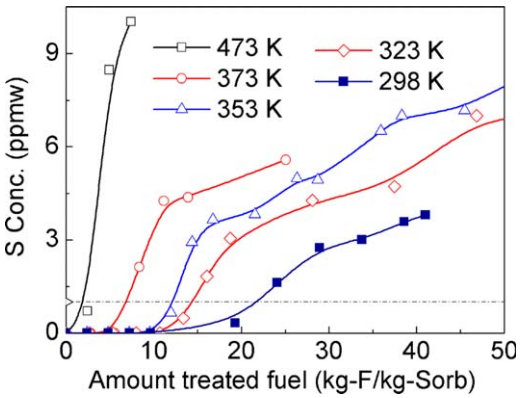

Figure 7. Breakthrough curves for sulfur compounds from the diesel fuel over the $Ti_{0.9}Ce_{0.1}O_2$ adsorbent with 10 cc/min (1.67 E − 7 m^3/s) of air flow at different temperatures.

[Color figure can be viewed in the online issue, which is available at wileyonlinelibrary.com.]

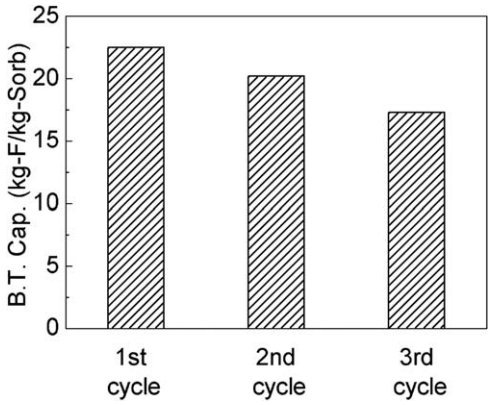

Figure 8. Breakthrough capacity of the $Ti_{0.9}Ce_{0.1}O_2$ adsorbent in the first three regeneration cycles by oxidative air treatment at 673 K.

Figure 9 shows the Ce $M_{4,5}$-edge XANES spectra of regenerated $Ti_{0.9}Ce_{0.1}O_2$ (from the 3rd cycle) in comparison to the fresh one. M5/M4 ratio (indicating Ce^{3+} ratio) of $Ti_{0.9}Ce_{0.1}O_2$ decreased to 0.868 from 0.889 after three regeneration cycles. The decreased percentage of trivalent Ce^{3+} on the $Ti_{0.9}Ce_{0.1}O_2$ surface may cause the formation of a lower number of surface active oxygen-vacancy sites for oxygen activation and sulfur oxidation, resulting in lower adsorption capacity after regeneration as shown in Figure 8. The results further consolidate that the reduced centers of Ce^{3+} on the $Ti_{0.9}Ce_{0.1}O_2$ surface can be critical for air-promoted ADS. The loss of active sites on the $Ti_{0.9}Ce_{0.1}O_2$ surface can be due to the agglomeration of metal oxide particles during regeneration at a high temperature. Alternatively, sulfur species may be retained on the regenerated $Ti_{0.9}Ce_{0.1}O_2$ after oxidative air treatment, which may form metal sulfate[24] and deactivate the catalytic sites for cyclic air-promoted ADS. Further mechanistic studies are needed to understand the deactivation/regeneration chemistry of the Ti-Ce mixed metal oxides.

Conclusions

Air-promoted ADS of commercial low-sulfur diesel fuel over Ti-Ce mixed metal oxides was examined. Sulfoxide species was identified to be formed over $Ti_{0.9}Ce_{0.1}O_2$ adsorbent during catalytic air-promoted ADS. Sulfoxides adsorbed on the adsorbent through a stronger R_2SO-M interaction rather than R_2S-M interaction, resulting in a significantly enhanced ADS capacity. Additionally, sulfoxides also minimize the steric hindrance effect by moving the thiophenic ring further away from the surface. Ce-XANES characterization indicates increased amounts of reduced Ce^{3+} sites by doping Ce into TiO_2, which may contribute to the creation of active O-vacancy sites for O_2 activation and sulfur oxidation. Air promotes ADS more at a lower temperature, and the $Ti_{0.9}Ce_{0.1}O_2$ adsorbent can be regenerated via oxidative air treatment. The decreased amount of reduced Ce^{3+} sites in the $Ti_{0.9}Ce_{0.1}O_2$ adsorbent contributes to partial loss of ADS capacity after regeneration, which should be taken into account in the future for improved design of air-promoted ADS adsorbents. The adsorbent studied not only minimizes the energy requirement but also eliminates the need for hydrogen and other sacrificial agents for oxidation keeping the costs low. At this stage of development, the air-promoted ADS process could be a complementary technique to HDS in the refineries to produce zero-ppm sulfur fuel while avoiding major reconstruction and capital costs.

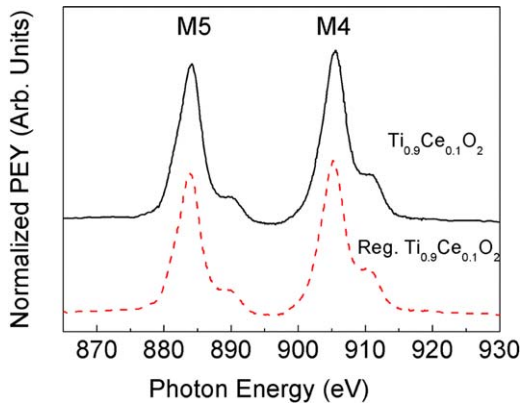

Figure 9. Ce $M_{4,5}$-edge XANES spectra of freshly prepared $Ti_{0.9}Ce_{0.1}O_2$, and regenerated $Ti_{0.9}Ce_{0.1}O_2$ (from the third regeneration cycle).

[Color figure can be viewed in the online issue, which is available at wileyonlinelibrary.com.]

Acknowledgments

This work was collectively supported by the National Energy Technology Laboratory of the US Department of Energy through grant DE-NT0004396, the US Office of Naval Research through grant N00014-06-1-0158, and the US Environmental Protection Agency-US National Science Foundation Joint TSE Program through grant R831471. XANES experiments conducted on U7A Beamline at the National Synchrotron Light Source (Brookhaven National Laboratory) was supported by the U.S. Department of Energy, Office of Basic Energy Sciences, under Contract DE-AC02-98CH10886. Use of the Advanced Photon Source, an Office of Science User Facility operated for the U.S. Department of Energy (DOE) Office of Science by Argonne National Laboratory, was supported by the U.S. DOE under Contract No. DE-AC02-06CH11357. Jing Xiao gratefully acknowledge the research grants from the National Natural Science Foundation of China (21306054), Guangdong Natural Science Foundation (S2013040014747), and PetroChina Innovation Foundation.

Literature Cited

1. Yang RT, Wang Y, Heinzel JM. Desulfurization of jet fuel by pi-complexation adsorption with metal halides supported on MCM-41 and SBA-15 mesoporous materials. *Chem Eng Sci*. 2008;63:356–365.
2. Song CS. Fuel processing for low-temperature and high-temperature fuel cells—challenges, and opportunities for sustainable development in the 21st century. *Catal Today*. 2002;77:17–49.
3. Song CS. An overview of new approaches to deep desulfurization for ultra-clean gasoline, diesel fuel and jet fuel. *Catal Today*. 2003;86:211–263.
4. Song CS, Ma XL. New design approaches to ultra-clean diesel fuels by deep desulfurization and deep dearomatization. *Appl Catal B*. 2003;41:207–238.
5. Velu S, Ma XL, Song CS. Selective adsorption for removing sulfur from jet fuel over zeolite-based adsorbents. *Ind Eng Chem Res*. 2003;42:5293–5304.
6. Ma XL, Sprague M, Song CS. Deep desulfurization of gasoline by selective adsorption over nickel-based adsorbent for fuel cell applications. *Ind Eng Chem Res*. 2005;44:5768–5775.

7. Hernandez-Maldonado AJ, Yang FH, Qi G, Yang RT. Desulfurization of transportation fuels by pi-complexation sorbents: Cu(I)-, Ni(II)-, and Zn(II)-zeolites. *Appl Catal B*. 2005;56:111–126.
8. Yang RT, Hernandez-Maldonado AJ, Yang FH. Desulfurization of transportation fuels with zeolites under ambient conditions. *Science*. 2003;301:79–81.
9. Favre-Reguillon A, Sevignon M, Rocault M, Schulz E, Lemaire M. Deep desulfurization of diesel feedstock by selective adsorption of refractory sulfur compounds. *Ind Eng Chem Res*. 2008;47:9617–9622.
10. Matzger AJ, Cychosz KA, Wong-Foy AG. Liquid phase adsorption by microporous coordination polymers: removal of organosulfur compounds. *J Am Chem Soc*. 2008;130:6938–6939.
11. Matzger AJ, Cychosz KA, Wong-Foy AG. Enabling cleaner fuels: desulfurization by adsorption to microporous coordination polymers. *J Am Chem Soc*. 2009;131:14538–14543.
12. Sentorun-Shalaby C, Saha SK, Ma XL, Song CS. Mesoporous-molecular-sieve-supported nickel sorbents for adsorptive desulfurization of commercial ultra-low-sulfur diesel fuel. *Appl Catal B*. 2011; 101:718–726.
13. Wang LY, Yang RT, Sun CL. Graphene and other carbon sorbents for selective adsorption of thiophene from liquid fuel. *AIChE J*. 2013;59:29–32.
14. Li W, Liu Q, Xing J, Gao H, Xiong X, Li Y, Li X. High-efficiency desulfurization by adsorption with mesoporous aluminosilicates. *AIChE J*. 2007;53:3263–3268.
15. Li W, Tang H, Zhang T, Li Q, Xing J, Liu H. Ultra-deep desulfurization adsorbents for hydrotreated diesel with magnetic mesoporous aluminosilicates. *AIChE J*. 2010;5:1391–1396.
16. Xiao J, Li Z, Liu B, Xia QB, Yu MX. Adsorption of benzothiophene and dibenzothiophene on ion-impregnated activated carbons and ion-exchanged Y zeolites. *Energy Fuels*. 2008;22:3858–3863.
17. Xiao J, Bian GA, Zhang W, Li Z. Adsorption of dibenzothiophene on Ag/Cu/Fe-supported activated carbons prepared by ultrasonic-assisted impregnation. *J Chem Eng Data*. 2010;55:5818–5823.
18. Alvarez-Rodriguez R, Clemente-Jul C. Hot gas desulphurisation with dolomite sorbent in coal gasification. *Fuel*. 2008;87:3513–3521.
19. Konttinen JT, Zevenhoven CAP, Hupa MM. Hot gas desulfurization with zinc titanate sorbents in a fluidized bed. 2. Reactor model. *Ind Eng Chem Res*. 1997;36:2340–2345.
20. Tamhankar SS, Hasatani M, Wen CY. Kinetic-studies on the reactions involved in the hot gas desulfurization using a regenerable iron-oxide sorbent .1. reduction and sulfidation of iron-oxide. *Chem Eng Sci*. 1981;36:1181–1191.
21. Xiao J, Sitamraju S, Chen YS, Janik MJ, Song CS. Air-promoted adsorptive desulfurization (ADS) over $Ti_{0.9}Ce_{0.1}O_2$ mixed oxides from diesel fuel under ambient conditions. *ChemCatChem*. 2013;5: 3582–3586.
22. Watanabe S, Ma XL, Song CS. Characterization of structural and surface properties f nanocrystalline TiO_2-CeO_2 mixed oxides by XRD, XPS, TPR, and TPD. *J Phys Chem C*. 2009;113:14249–14257.
23. Kim JH, Ma XL, Zhou AN, Song CS. Ultra-deep desulfurization and denitrogenation of diesel fuel by selective adsorption over three different adsorbents: a study on adsorptive selectivity and mechanism. *Catal Today*. 2006;111:74–83.
24. Chen YS, Xie C, Li Y, Song CS, Bolin TB. Sulfur poisoning mechanism of steam reforming catalysts: an X-ray absorption near edge structure (XANES) spectroscopic study. *Phys Chem Chem Phys*. 2010;12:5707–5711.
25. Ravel B, Newville M. ATHENA, ARTEMIS, HEPHAESTUS: data analysis for X-ray absorption spectroscopy using IFEFFIT. *J Synchrotron Radiat*. 2005;12:537–541.
26. Chen CT, Sette F. Performance of the dragon soft-X-ray beamline. *Rev Sci Instrum*. 1989;60:1616–1621.
27. Kim K, Zhu PY, Li N, Ma XL, Chen YS. Characterization of oxygen containing functional groups on carbon materials with oxygen K-edge X-ray absorption near edge structure spectroscopy. *Carbon*. 2011;49:1745–1751.
28. Kresse G, Furthmuller J. Efficient iterative schemes for ab initio total-energy calculations using a plane-wave basis set. *Phys Rev B*. 1996;54:11169–11186.
29. Kresse G, Furthmuller J. Efficiency of ab-initio total energy calculations for metals and semiconductors using a plane-wave basis set. *Comput Mater Sci*. 1996;6:15–50.
30. Kresse G, Furthmuller J. Ab initio molecular-dynamics for liquid-metals. *Phys Rev B*. 1993;47:558–561.
31. Kresse G, Joubert D. From ultrasoft pseudopotentials to the projector augmented-wave method. *Phys Rev B*. 1999;59:1758–1775.
32. Perdew JP, Chevary JA, Vosko SH, Jackson KA, Pederson MR, Singh DJ, Fiolhais, C. Atoms, molecules, solids, and surfaces—applications of the generalized gradient approximation for exchange and correlation. *Phys Rev B*. 1992;46:6671–6687.
33. Monkhorst HJ, Pack Venue JD. Special points for Brillouin-zone integrations. *Phys Rev B*. 1976;13:5188–5192.
34. Grimme S. Semiempirical GGA-type density functional constructed with a long-range dispersion correction. *J Comput Chem*. 2006;27: 1787–1799.
35. Sitamraju S, Janik MJ, Song CS. Selectivity of adsorption of thiophene and its derivatives on titania anatase surfaces: a density functional theory study. *Top Catal*. 2012;55:229–242.
36. Francl MM, Pietro WJ, Hehre WJ. Representation of electron densities. 1. sphere fits to total electron density surfaces. *J Am Chem Soc*. 1984;106:563–570.
37. Almarri M, Ma XL, Song, CS. Selective adsorption for removal of nitrogen compounds from liquid hydrocarbon streams over carbon- and alumina-based adsorbents. *Ind Eng Chem Res*. 2009;48:951–960.
38. Almarri M. *Selective adsorption for removal of nitrogen compounds from hydrocarbon streams over carbon-based adsorbents*. PhD Dissertation, The Pennsylvania State University, Pennsylvania, 2009.
39. Guo JH, Janik MJ, Song CS. Density functional theory study on the role of ceria addition in TixCe1-xO2 adsorbents for thiophene adsorption. *J Phys Chem C*. 2012;116:3457–3466.
40. Jalilehvand F. Sulfur: not a "silent" element any more. *Chem Soc Rev*. 2006;35:1256–1268.
41. Yagci O. The M4,5 photoabsorption spectra of cerium in CeO_2 and oxidation of metallic cerium. *J Phys C: Solid State Phys*. 1986;19: 3487–3495.
42. Skala T, Tsud N, Orti MAN, Mentes TO, Locatelli A, Prince KC, Matolin V. In situ growth of epitaxial cerium tungstate (100) thin films. *Phys Chem Chem Phys*. 2011;13:7052–7058.
43. Li H, Wang H, Gong X, Guo Y, Guo Y, Lu G, Hu P. Multiple configurations of the two excess 4f electrons on defective CeO_2(111): origin and implications. *Phys Rev B*. 2009;79:193401.
44. Huang M, Fabris S. Role of surface peroxo and superoxo species in the low-temperature oxygen buffering of ceria: density functional theory calculations. *Phys Rev B*. 2007;75:081404R.
45. Xiao J, Wang X, Fujii M, Yang Q, Song CS. A novel approach for ultra-deep adsorptive desulfurization of diesel fuel over TiO_2-CeO_2/MCM-48 under ambient conditions. *AIChE J*. 2013;59:1441–1445.

Manuscript received July 18, 2014, and revision received Sep. 5, 2014.